Journal of Soils and Sediments
https://doi.org/10.1007/s11368-023-03594-9

SOILS, SEC 1 • SOIL ORGANIC MATTER DYNAMICS AND NUTRIENT CYCLING • RESEARCH ARTICLE

Evaluation of swelling properties of different biochar-doped hydrogels

Yağmur Uysal[1] · Zeynep Görkem Doğaroğlu[1] · Zehranur Çaylali[1] · Mehmet Nuri Makas[1]

Received: 24 February 2023 / Accepted: 23 June 2023

Abstract

Purpose Nowadays, there is an increasing interest in hydrogel production and usability at different fields especially agricultural applications since biodegradable polymeric hydrogels can enhance the water retention capacity of soil and the nutritional status of plants. This work aimed to determine the biochar-doped hydrogel production and their swelling properties in deionized water, tap water, and saline water 0.5% and 1%. It was also evaluated that the phytotoxicological impacts on wheat seeds.

Method The hydrogel production was realized using PVA-SA polymers and it contained different amounts of biochar from vineyard pruning wastes, dry leaves, and compost. The characterization analysis of the synthesized biochars, biochar-doped hydrogels, and raw hydrogels was realized by FT-IR and SEM. The swelling capacity, time-dependent swelling kinetics, re-swelling properties, and wheat germination and root-shoot elongation impacts of synthesized hydrogels were evaluated.

Results and conclusion The hydrogels contained three types of biochar and showed different swelling properties in different aqueous media. The maximum and the minimum swelling capacity was determined in saline water (0.5% and 1%) and deionized water, respectively. The maximum time-dependent swelling capacity was determined at 0.1% leaf (as 193.2%) and vine pruning (as 142.6%) biochar-doped hydrogels, and 0.2% compost (128.93%) biochar-doped hydrogels. The phytotoxicological test results showed that the shoot length decreased by 42.06% for 0.4% LBHG, 27.5% for 0.4% VBHG, and 23.91% for 0.2% CBHG treatment. For hydrogel production, the threshold and eco-toxicological properties should be well determined for hydrogel and hydrogel additives.

Keywords Biochar · Climate change · Compost · Hydrogel · Vine

1 Introduction

One of the main contributors to the environment's pollution has been identified as the negligent and improper use of fertilizers. Two significant problems that have persisted for a very long time in agricultural practices are excessive irrigation and the ineffectiveness of quick fertilizer (Du et al. 2015). According to estimates from two sources, erosion and subsurface soil have caused 40 to 60% of irrigation water to be lost (Laird et al. 2010). Such losses can be managed by encapsulating fertilizer granules using various biodegradable superabsorbent polymers (Zhang et al. 2020). Utilizing these biodegradable polymers allows for the gradual release of mineral nutrients, as well as the efficient uptake of those minerals by crops, which reduces soil and water pollution (Li and Chen 2018a). Additionally, they can reduce the frequency of fertilizer applications and important negative effects such over dosage (Liu et al. 2019).

Biochar (BC) is simply carbon-rich, extremely porous materials produced by the pyrolysis of biomass under anoxic conditions using temperatures ranging from 350 to 900 °C (Das et al. 2023). Gasification, hydrothermal carbonization, and pyrolysis (slow and quick) can all be used to transform waste biomass into biochar (Gaur et al. 2022). The composition of the biochar changes as the pyrolysis conditions are changed (Al-Wabel et al. 2013). The kind of feedstock and pyrolysis circumstances affect the biochar's chemical composition. In general, higher levels of nitrogen, sulfur, calcium, magnesium, phosphorus, larger surface area, and higher cation exchange capabilities are associated with a slower pyrolysis process. This is due to the biochar losing

Responsible editor: Zhaoliang Song

✉ Zeynep Görkem Doğaroğlu
gorkemdogaroglu@gmail.com

[1] Engineering Faculty, Environmental Engineering Department, Mersin University, Mersin, Turkey

Published online: 05 July 2023

its easily decomposable and volatile components, such as oxygen, hydrogen, nitrogen, total phosphorus, and sulfur, during the slow pyrolysis process (Lehmann and Joseph 2015). Pyrolyzed biochar is also very effective at immobilizing heavy metals in soil by ion exchange, co-precipitation, physical adsorption, inner-sphere complexation, electrostatic cationic attraction, and electrostatic surface complexation (Singh et al. 2020). A type of carbonaceous material is created when biomass is pyrolyzed in a course, simple, and industrial-scale manner with little oxygen (Wang et al. 2020). Additionally, biochar can be used in building, anaerobic digestion, animal husbandry, water treatment, composting, soil remediation, energy storage, and agronomy (Osman et al. 2022). Because of its potential agronomic, financial, and environmental advantages, BC has the potential to function as a promising soil conditioner (Tu et al. 2020). Complex organic matter makes up around 40–75% of the carbon in BC, and it is difficult for microorganisms to break this material down (Tan et al. 2015).

Cross-linked polymers to which hydrophilic functional groups are attached form hydrogels (Godiya et al. 2019; Li and Chen 2020). Hydrogels are potential repositories for surplus water and nutrients in agricultural soils due to their distinctive porous architectures and variety of hydrophilic functional groups. Conventional polyacrylamide hydrogels were shown to be capable of holding 326 times their dry weight in distilled water, according to a previous study (Kim et al. 2010). They have been applied as soil amendments to maximize efficient water use in crop growing (Suresh et al. 2018) The biodegradable carrier hydrogels can store a large amount of nutrients, release them gradually into the soil solution, and maintain nutrient concentration for a longer period under ideal circumstances.

The use of biochar as a bio-sorbent for amending contaminated soils has also drawn interest recently for similar reasons. Biochar has a large surface area and is made up of a variety of functional groups (Wang et al. 2009). However, there are considerable drawbacks to using pure BC as a soil amendment, including its limited capacity for adsorption, its difficulty in adsorbing different contaminants, and its facilitation of the mobility of particular heavy metals (Feng et al. 2017). To increase its environmental applicability, BC must be functionalized and modified into a sophisticated composite. The hydrogel-biochar composite typically functions by absorbing mineral nutrients into their cross-linked structure, holding them firmly, and delaying disintegration (Das et al. 2021). Because it is made from industrial wastes, animal hair, and agricultural wastes, it is less expensive than many other materials (Li et al. 2019). In another way, building biochar into a three-dimensional structure is thought to be a possible solution to the problem of separation and regeneration of biochar particles. The advantages of hydrogel-based soil additives in terms of bettering water-holding capacity and stabilizing soil structure have recently received increased attention (Ma et al. 2020). A promising soil supplement for both increasing nitrogen utilization effectiveness and immobilizing heavy metals in soil is a composite made of hydrogel and BC. To the best of our knowledge, only a few research has amended soil using the hydrogel-BC combination (An et al. 2020). Organic matter can help soils by increasing their structure, nutritional content, and chemical properties (Rahman et al. 2017). In this study, biochar was obtained from different agricultural wastes (vineyard pruning wastes, dry leaves (redbud tree leaves) collected from the campus area) and compost produced from kitchen wastes released during meal preparation from the cafeterias and dining halls in the main campus of Mersin University.

The main aim of this study is to produce an efficient and cost-effective biochar-hydrogel composite using the polymerization technique. The produced biochar-hydrogel composites will exhibit great water retention and nitrogen release in the soil when added to soil in agricultural applications. The biochar in the biochar-hydrogel composite is expected to retain more water than the non-biochar composite. At the same time, different biochar dosages will change the structural architecture of the composite. In this study, biochars were synthesized from agricultural wastes (dry redbud leaves and vine pruning wastes) containing cellulose and hydrogel composites containing these biochars (LB, VB) were also prepared. An important innovation of our study is the use of carbon, nitrogen, and phosphorus, that are, the nutritional elements contained in the compost produced from the co-mixture of fruit and vegetable wastes (cellulosic mixture), by transferring them to biochars (CB) obtained from these cellulosic wastes and converting them into a useful product of hydrogel (CBH). There is no study in the literature examining the swelling properties of compost/biochar-added hydrogels by placing the compost as biochar into the hydrogel and its effects on the plant. The characterization processes such as identification, verification, swelling properties, and surface structure analysis of the synthesized biochars (VB, CB, LB), biochar doped (VBHG, CBHG, and LBHG), and raw hydrogels were characterized by techniques such as Fourier transform infrared spectroscopy (FT-IR) and scanning electron microscopy (SEM). The swelling capacities of biochar/hydrogel composites in deionized water, tap water, and saline water (0.5% and 1%), and time-dependent swelling behavior of hydrogels were also determined.

2 Materials and method

2.1 Biochar production and chemical analyses of the materials

Biochar-doped hydrogels were synthesized from obtained biochars and characterizations of both biochar and synthesized hydrogels were also carried out. The swelling properties of these hydrogels, their water-holding capacity in aqueous and soil environment, swelling kinetics, and all their features have been investigated. The biomass of vine pruning wastes (VB) (5 cm), dry compost (CB), and dry redbud leaves (LB) from garden was oven dried (65 °C, 48 h) and pyrolyzed at high temperature via slow pyrolysis method (500 °C hold temperature, 4 h and heat rate 10 °C/min) using pyrolysis reactor (UnitermLab). The prepared biochar was collected from the reactor and keep in the desiccator until reach to room temperature. They were grounded, sieved (0.2 mm), and stored for further analyses. Elemental analyses of produced biochars to determine C, H, and N content % were made by Eurovector, EA3000-Single Analyzer. The pH values of the biochar samples were determined after extraction with 0.01 M $CaCl_2$ (w/v = 1/5) by pH meter (Thermo Scientific, Orion Star-A111). The electrical conductivity values (EC) were measured by using a multiparameter meter (Hach, HQ440d) after filtration of biochar/deionized water solution (w/w = 1/10) according to Das and Ghosh (2022). In the study, biochar was also produced from the compost produced in a rotating drum compost machine for 2 months by using vegetable and fruit wastes, dry leaves, wood, etc., which are released during the food preparation stage in the cafeteria and meal saloons in the Mersin University Campus. The chemical composition of matured and dried compost used in biochar production was given in Table 1.

Table 1 The chemical composition of used compost samples (CB)

Parameter	Value
pH	7.64
EC (mS/cm)	1.75
Organic content (%)	78.59
Dry matter (%)	33.30
Humidity	11
Total N (kg/kgdw)	10
Total P (g/kgdw)	521
N (%)	3.13
C (%)	40.02
K (%)	0.61
Ca (%)	0.83
Mg (%)	0.44
C/N	12.78

2.2 Synthesis of biochar-doped hydrogels

The pure hydrogel beads were synthesized according to Putra and Lee (2020). Briefly, poly-vinyl alcohol (PVA) (5 g) and sodium alginate (SA) (5 g) were stirred in 100 mL of deionized water and were autoclaved for 30 min at 120 °C. Then, the solutions were dripped with a syringe into $CaCl_2$ (5% w/v) solution, which was stirred at 100 rpm and they were kept in $CaCl_2$ solution for a night to complete cross-linking. In order to obtain biochar-doped composite hydrogels after the autoclaving, a different amount of three types of biochars (0.1–0.2–0.4–0.8%) were added into the solution and mixed thoroughly. The homogeneous BC/PVA/SA solution were dripped into $CaCl_2$ to complete cross-linking, like pure hydrogel beads. Finally, the obtained pure and BC/PVA/SA hydrogel beads were washed with deionized water to remove residual $CaCl_2$.

2.3 Characterization of BCs and BC composite hydrogels

The surface morphologies of the VB, CB, LB, VBHG, CBHG, and LBHG, and raw hydrogel beads were investigated by SEM using a Quanta 650 FEG produced by FEI, USA. The chemical bonds of the materials were analyzed using FT-IR spectra (FT/IR-6700, Jasco), in KBr pellet techniques in the range of 4000–500 cm^{-1}.

2.4 Swelling capacity of hydrogels in aqueous and soil media

The swelling capacity of synthesized hydrogels in aqueous media was determined according to Feng et al. (2017). For this purpose, synthesized hydrogel beads were left to dry at room temperature (25 °C) to complete the dehydration process (approx.. 5 days). After 2 days, 0.2 g of dried hydrogels (w_{dry}) were left in distilled water, tap water (pH 7.68 and 9.0), and saline water (0.5% and 1%) at room temperature for 4 days until the equilibrium swelling degree. The swelled hydrogel beads were removed from the water, slightly dried with wet filter paper, and weighed immediately ($w_{swelled}$). All treatments were conducted in 3 replicates. The equilibrium swelling ratio was calculated using Eq. (1):

$$\mathrm{ESR}(\%) = \frac{(\mathrm{Wswelled} - \mathrm{Wdry})}{\mathrm{Wdry}} \times 100 \quad (1)$$

To determine the swelling capacity (SC) in soil media, the experiments were conducted according to method given by Abdallah (2019). To compare the swelling capacity of hydrogels which different biochar type and amount, in the

free water and in the water-soil mixture, the 100-g sandy soil samples, 1 g hydrogels, and 1 g hydrogel + 100-g loamy sand soil were weighed and transported into permeable nylon bags. Then, the bags were immersed in a glass beaker filled with 2 L of tap water (pH 7.0) for 15 min. The swelling capacity of hydrogels was measured gravimetrically in the free water and in the water-soil mixture and calculated as follow (Eq. (2)). All treatments were conducted in 3 replicates.

$$SC = \frac{(\text{Wwet hydrogel} + \text{soil} - \text{Wwet soil})}{\text{Wdry hydrogel in mixture}} \quad (2)$$

The soil texture used in this study was loamy sand and the other properties were as pH: 7.37, electrical conductivity: 628 µs/cm, organic matter content 1.21%, lime 24%, clay (< 0.002 mm) 1.3%, silt (0.002–0.06 mm) 10%, sand (0.06–2 mm) 88%, saturation degree 33%, and salt 0.012 dS/m.

2.5 Time-dependent swelling behavior of hydrogels

The swelling kinetic experiments of raw and biochar composite hydrogels were conducted according to Liu and Huang (2016). For this purpose, 0.2-g dried composite hydrogels were left in distilled water, and they were weighed at different time interval (5–10–20–40–80–160–320 min) at room temperature. For the first measurement, the hydrogels were removed from water after 5 min, dried slightly with wet filter paper, and weighed immediately, and then, they were left into water again. This procedure was also applied for further minutes and the swelling kinetics were calculated for every time intervals by using Eq. (1). All treatments were conducted in 3 replicates.

2.6 Water diffusion model of hydrogels

Swelling kinetics and diffusion of the polymeric structures are explained using Fick's most fundamental law. Polymers' swelling dynamics can be calculated by using the Fick equation (Peppas et al. 2000; Zarzycki et al. 2010) as follows (Eq. (3)):

$$F = \frac{S_t}{S_e} = kt^n \quad (3)$$

where "F" represents the swelling fraction, "S_e" is the equilibrium swelling content of hydrogel, and "k" is the diffusion exponential of the solvent and is the constant that changes according to the gels' network structure. The parameter of "n" must be known to determine the type of diffusion. The slope of the lines obtained by linearizing the *lnF-lnt* graphs data from the calculated *F* values (swell fraction) is used to estimate the "n" diffusion exponent. The coefficient of diffusion is a key variable in the analysis of the swelling kinetics. The coefficient of "D" for cylindrical objects can be calculated using the equation (Dengre et al. 2000) that results from the arrangement of Fick's II law (Eq. (4)).

$$D = \pi r^2 (k/4)^{1/n} \quad (4)$$

where "D" represents the coefficient of diffusion as "$m^2\ s^{-1}$" and "r" represents the swollen gels radius as "m."

2.7 Re-swelling capacity of hydrogels

After the hydrogels were dried for 2 days at room temperature, 0.2 g of dry hydrogels was left in deionized water for 80 min. Then, they were slightly dried with wet filter paper, weighed, and dried at 80 °C in an oven. They were left again deionized water for 80 min, weighed, and dried at 80 °C. This cycle was conducted 3 times and with 3 replicates (Abdallah 2019).

2.8 Seed germination experiments

To determine the phytotoxicological effects of synthesized hydrogels on wheat, the seed germination tests were realized, according to Doğaroğlu (2019). The wheat seeds were used in this study were purchased from Mersin, Turkey. Clearly, the wheat seeds (*Triticum aestivum* L. İkizce-96) were sterilized with 70% ethanol and 5% sodium hypochlorite solution, respectively, and they were rinsed with deionized water 5 times for 5 min. After the sterilization process, the 10 wheat seeds with uniform size were placed on a double layer of filter paper in Petri dishes (100 × 20 mm). Then, 3 mL of deionized water was added to Petri dishes and 2 g of raw and biochar-doped hydrogels was placed on seeds. The hydrogels were used as water supplier for the seed germination process. For the control groups, hydrogels were not added to Petri dishes and only 5 mL of deionized water was used for the germination process. The Petri dishes were kept in dark at 25 °C for 7 days. All treatments were conducted in three replicates. After the germination process (7 days), the number of germinated seeds (radicle length > 5 mm) was counted and the germination percentage (%) was calculated (Eq. (5)) (Doğaroğlu et al. 2019). The seedling vigor index (SVI) was also calculated depending on the germination percentage and average root and shoot length according to Doğaroğlu et al. (2019) (Eq. (6)).

$$\text{Germination Percentage (GP)} = \frac{\text{Total number of germinated seeds}}{\text{Total number of tested seeds}} \times 100 \quad (5)$$

$$\text{Seedling Vigor Index(SVI)} = \text{GP}(\%) \times (\text{Root lenght} + \text{Shoot Lenght}) \quad (6)$$

2.9 Statistical analyses

The statistical analyses of the results were performed using ANOVA with the LSD test. SPSS Statistic program version 20 was used in the calculations. The significance of difference for all measurements was calculated by the least significant difference, LSD, $p < 0.05$.

3 Results and discussion

3.1 Characterization of biochar and biochar-hydrogel composites

The surface morphologies of biochar (VB, CB, and LB) and biochar-hydrogel composites (VBHG, CBHG, and LBHG)

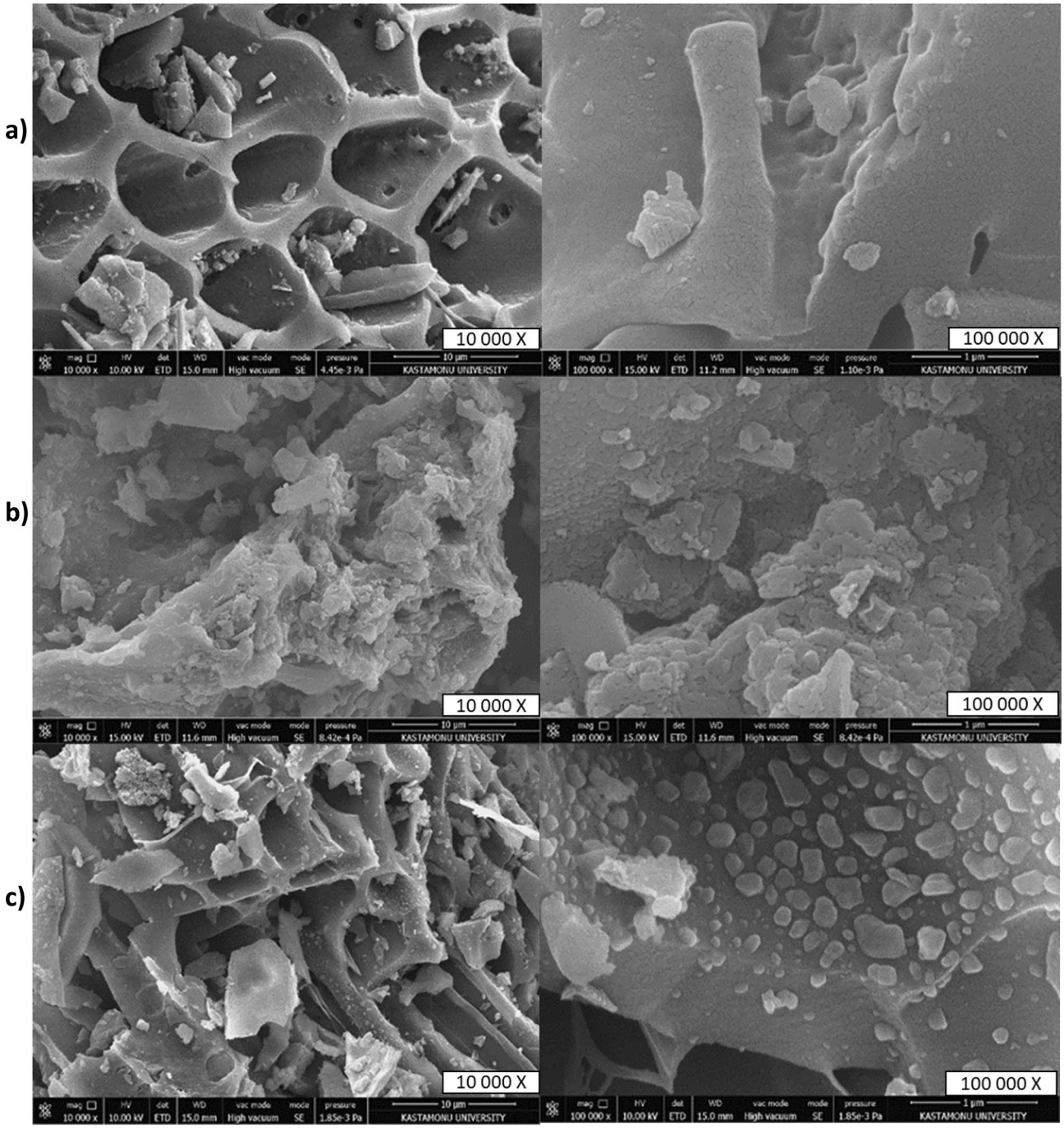

Fig. 1 SEM images of biochar derived from **a** vine (VB), **b** compost (CB), and **c** leaf (LB)

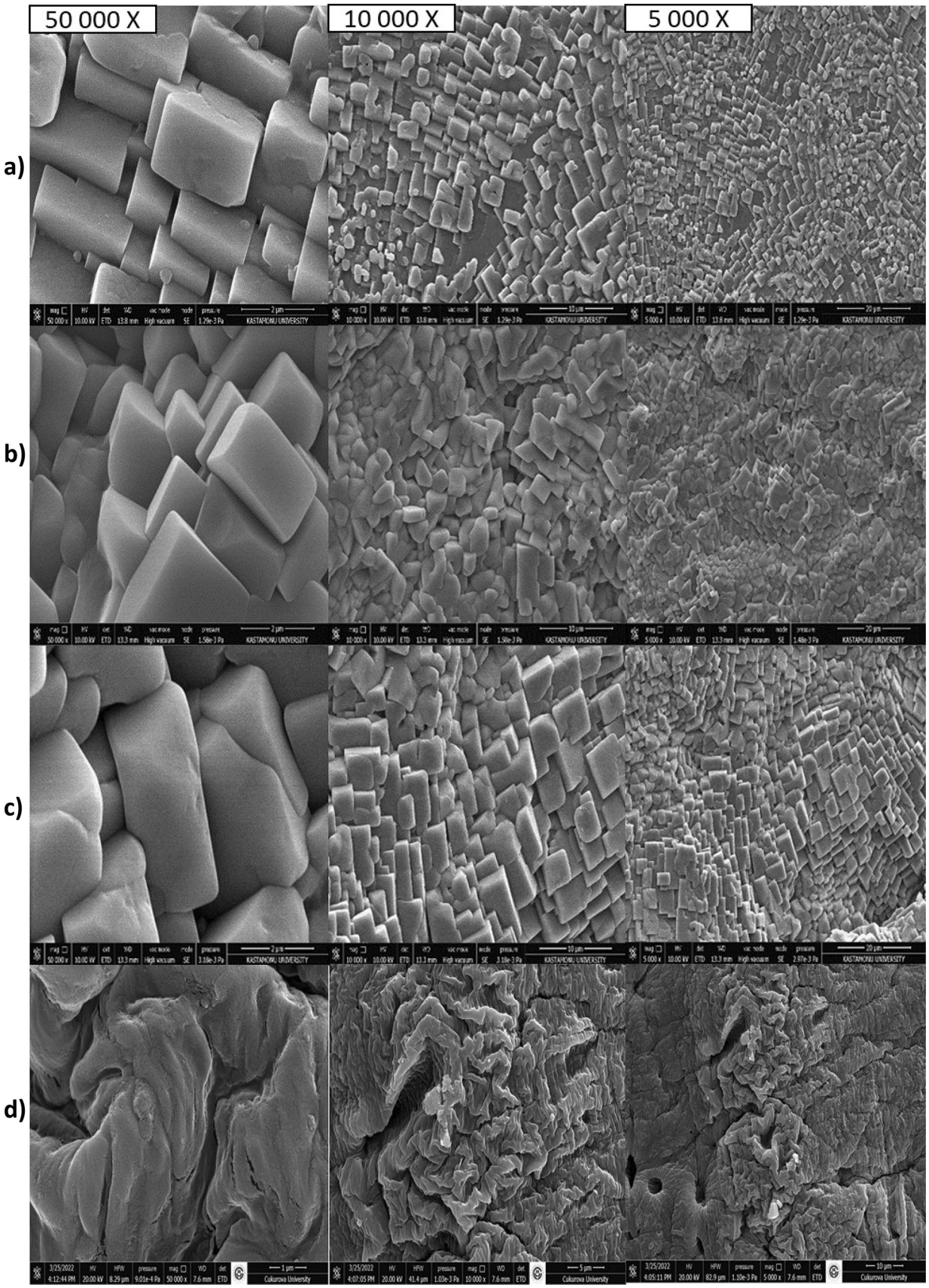

Fig. 2 SEM images of **a** VB-doped hydrogels (VBHG), **b** CB-doped hydrogels (CBHG), **c** LB-doped hydrogels (LBHG), and **d** raw hydrogels

were determined and shown in Figs. 1 and 2, respectively. SEM images of VB, CB, and LB biochar showed significant differences between samples. SEM micrographs of the produced biochar and especially LB showed different pore structures as micro-, macro-, and mesopores. However, the biochars of VB and LB produced at 500 °C developed a honeycomb-like shape with holes in the cylindrical structure. It can be seen under the microscope that the three-biochar form many regularly spaced pores. It is possible to detect a consistent pattern of small vertical blocks on the surfaces of VB and LB biochar. The particles and structures of biochar are very porous, hollow, spherical, and well organized (Fig. 1a and c). The structures had thick walls and resembled hexagonal voids in a honeycomb structure, exhibiting a robust and non-fragile appearance. The only biochar that was structurally different from the others was compost biochar. It was observed that CB has a porous structure and rough surfaces. The structure of CB exhibited a bulky and microporous structure.

In Fig. 2, SEM images of the hydrogels contained in these biochar samples are given. SEM images of the hydrogels containing the three-biochar revealed very interesting structures (Fig. 2a–c). Similarities of these SEM images have not been found in the literature. It is an interesting result that these structures are brick-like, highly ordered cubic structures. Three-dimensional cubic structures are regularly attached to each other. Only the cubic structures of CB showed a more cohesive and interlocked bulk appearance (Fig. 2b). Raw hydrogels (Fig. 2d) were not used to determine these cubic forms. Raw hydrogel surfaces revealed the structure of wrinkles. The SEM images demonstrated how adding biochar to hydrogels affected their surface shape, and it was found that biochar was present not only within the hydrogels themselves but also on the surface. As a result of the hydrophilic group formations on the surface, this result affected the hydrogels' ability to swell.

FT-IR spectra of biochar were shown in Fig. 3a. When the FT-IR spectra of biochar are examined, it can be seen from the different spectrum that the FT-IR spectra of the VB and LB also show similarity due to their structural similarities, while the compost has quite different functional bonds. More clear information about chemical bonding, peak position, and intensity from Fig. 3a was shown in also Table 2. When studying the organic components of biochar, the majority of FT-IR characteristics comes from organic functional groups. The peak at 3667 cm^{-1} in the CB spectra would be expected from organic O–H stretching with contribution from any water molecule that may remain in the sample (Armynah et al. 2019). The vibration of C = O stretching of a cyclic and acid anhydride is ascribed to weak intensity at 2100–2070 cm^{-1} due to thermal degradation with substantial loss of oxygen atoms and produced CO_2 gas (Das and Ghosh 2022). The aromatic group from lignin gives to C = C asymmetric stretching at 1566 cm^{-1} corresponding to the sp2-hybridization bonding of carbon atoms (Chen et al. 2015). C-H bending modes appeared at 870 cm^{-1} in all biochar. The transmittance at 1400 cm^{-1} is due to the methyl group (–CH_3) stretching vibration as discussed by Coates (2006); Jipa et al. (2012); and Siipola et al. (2018). The transmittance at 1050 cm^{-1} is due to the occurrence of aliphatic ether C = O and alcohol (Mary et al. 2016). The peak observed at 870–710 cm^{-1} reveals alkynes with C-H bending being present (Ray et al. 2020).

The most crucial functional groups in the BCH composites and raw hydrogel samples were validated by the FT-IR graphs in Fig. 3b and c, and more clear information was shown in also Table 2. The FT-IR revealed that the vibration of functional groups on the superabsorbent hydrogel fragments was controlled by the intermolecular relationships. The FT-IR peaks found at 3380 cm^{-1} was due to vibration bands of -OH stretching (Coates 2006; Siipola et al. 2018; Sánchez-Borrego et al. 2022). The -CH_3 and -CH_2 groups were present at the peak at 2920 cm^{-1}, which was caused by C-H stretching vibrations of aliphatic groups (Kang et al. 2012; Moretti et al. 2014; Shivakumara and Demappa 2019). Similarly, the peak found at 1620 cm^{-1} showed the C = O stretching of PVA (Korbag and Saleh 2016; Helmiyati and Aprilliza 2017). The FT-IR peaks of biochar-based hydrogels illustrated the multiple peaks in the region of 490–1420 cm^{-1} (Coates 2006; Jipa et al. 2012; Siipola et al. 2018). The C = O stretching band, as a medium-intensity peak at 1420 cm^{-1}, revealed properties of both SA and PVA (Korbag and Saleh 2016). It is evident that when SA is added, the hydroxyl stretches bands widen significantly, providing strong evidence that a hydrogen bond can form between the hydroxyl groups of PVA and this SA group (raw hydrogel). The peak at about 1017 cm^{-1} attributed to C–O–C stretching bond from sodium alginate in hydrogel (Isawi 2020). The stretching vibrations of hydrogen-bonding C–OH groups and aromatic C–H stretching vibrations can be observed at 1080 cm^{-1} and 820 cm^{-1} in FT-IR spectra, respectively (Coates 2000; Thayumanavan et al. 2014; Ray et al. 2020). C = O stretching bonds originating from sodium alginate also showed themselves at approximately 490 cm^{-1} (Isawi 2020). Also, Table 3 shows the elemental compositions of the produced vine, compost, and leaves' biochar.

3.2 Swelling capacity of hydrogels in different aqueous media

The swelling ratios of the synthesized hydrogels from PVA/SA/biochar in different aqueous media (pure water, tap water-pH 7.0, tap water-pH 9.0, 1% saline water, and 0.5% saline water) were determined. It is important to evaluate the swelling capacities in different media for agricultural application of hydrogels. The swelling capacity of leaves

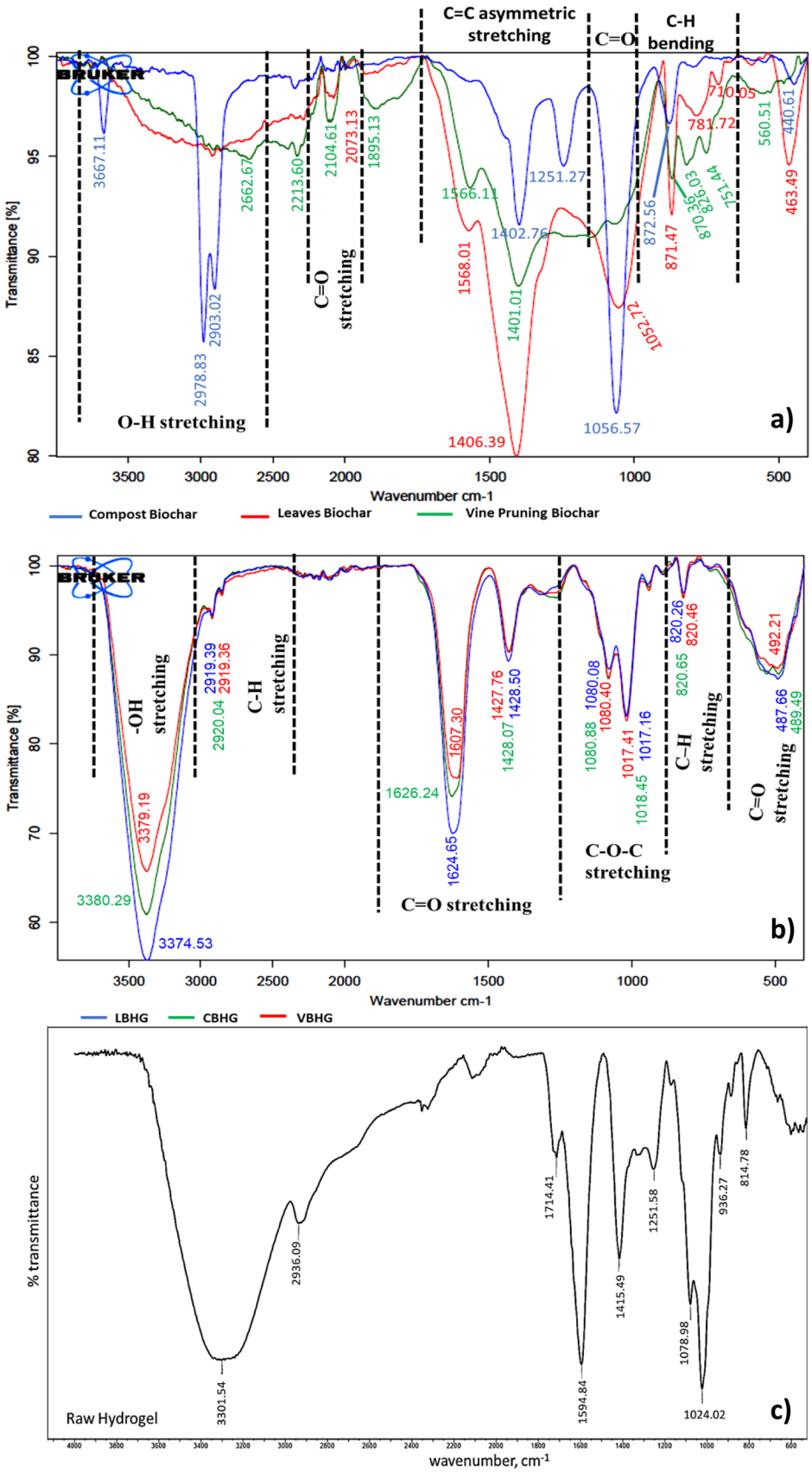

Fig. 3 FT-IR spectrums of synthesized **a** CB, LB, and VB; **b** VBHG, CBHG, and LBHG; and **c** raw hydrogel

Table 2 The functional groups in the VB, CB, LB, and biochar-doped hydrogels

VB	CB	LB	VBHG	CBHG	LBHG	Groups/compound class	Ref
-	3667	-	3379	3380	3374	-OH stretching vibration band	Coates (2006); Siipola et al. (2018); Armynah et al. (2019); Sánchez-Borrego et al. (2022)
2662	2978–2903	-	2919	2920	2919	C-H stretching for aliphatic (alkane/alkyl) groups	Kang et al. (2012); Moretti et al. (2014); Shivakumara and Demappa (2019)
2104	2086	2073	-	-	-	C = O stretching	Das and Ghosh (2022)
-	-	-	1607	1626	1624	C = O stretching	Korbag and Saleh (2016); Helmiyati and Aprilliza (2017)
1566	-	1568	-	-	-	C = C stretching in the aromatic ring	Chen et al. (2015); Ray et al. (2020)
1401	1402	1406	-	-	-	methyl group ($–CH_3$) stretching vibration	Coates (2006); Jipa et al. (2012); Siipola et al. (2018)
-	-	-	1427	1428	1428	C = O stretching	Korbag and Saleh (2016)
1244	1251	-	-	-	-	C = O stretching	Armynah et al. (2019)
1062	1056	1052	-	-	-	aliphatic ether C = O and alcohol	Mary et al. (2016)
-	-	-	1080	1080	1080	C-O stretching (primary alcohol)	Coates (2000); Thayumanavan et al. (2014)
-	-	-	1017	1018	1017	C–O–C stretching bond from sodium alginate	Isawi (2020)
870	872	871	-	-	-	C-H bending	Coates (2000)
826	-	-	820	820	820	aromatic C–H stretching vibration	Ray et al. (2020)
751	-	781–710	-	-	-	aromatic C–H stretching vibration	Ray et al. (2020)
-	-	-	492	489	487	C = O stretching bond from sodium alginate	Isawi (2020)

biochar-doped hydrogels (LBHG) was range from 39.7 to 63.5% at various concentrations of biochar. The minimum and the maximum swelling capacities of LBHG were determined in pure water and in 1% saline water, respectively. It was determined that the swelling capacity of LBHG in pure water was significantly decreased compared to raw hydrogels ($p < 0.05$). Also, the same trend was observed in tap water at pH 7.0 and 9.0, where the raw hydrogels swelled well compared to LBHG. In both tap waters, swelling capacity increased with increasing LB content in hydrogels at different pH values, but did not reach the value obtained in raw hydrogels (Fig. 4a). In addition, the maximum swelling capacity was observed in 1% saline water both in raw and LB-doped hydrogels. It was determined that increasing LB content in hydrogels caused increasing swelling capacity in 1% saline water (Fig. 4a). The maximum swelling capacity was determined as 556.60% in 1% saline water.

Table 3 The elemental compositions and physicochemical properties of the produced VB, CB, and LB

Biochar	Elemental composition (%)			pH	EC (µS/cm)
	C	**N**	**H**		
VB	79.319	0.357	1.265	9.04	990
CB	46.852	1.780	2.053	9.39	950
LB	52.349	0.293	1.775	9.29	910

The swelling capacity of hydrogels depends on the types and quantity of the additives in hydrogels, as well as the hydrogel's swelling media. The determined highest swelling capacity in saline media can be explained by salting-in effect and hygroscopic properties, which is known as the absorption of water by diffusion or concentrating water in hydrogels' walls (Aleid et al. 2022). The maximum swelling capacity of VBHG and CBHG was determined in saline water, like LBHG (Fig. 4b and c). The swelling properties of VBHG in different aqueous media, VBHG showed the minimum swelling capacity in pure water. Also, it significantly decreased with increasing vine pruning biochar content in hydrogels ($p < 0.05$). The raw hydrogels showed similar swelling trend in similar media, such as tap water pH 7.0 and 9.0 or 0.5% and 1% saline water (Fig. 4b). The highest swelling capacity was determined at the content of 0.2% VB content in hydrogel for almost all aqueous media. Besides in the saline water, the VBHG swelled good in tap water at pH 9.0. Cheng et al. (2015) synthesized and characterized different hydrogels in different media. The authors used different amount of cellulose, acrylic acid (AA), *N,N1*-methylenebisacrylamide (MBA), and potassium persulfate (KPS) to synthesized hydrogels. They showed that the hydrogels which include 1 g cellulose, 9 g AA, 0.8% MBA/AA, and 1.5% KPS/AA reached the maximum swelling capacity at pH 7.0, then the swelling capacity decreased because of the anion–anion repulsion in solution. It is seen that the increase in swelling

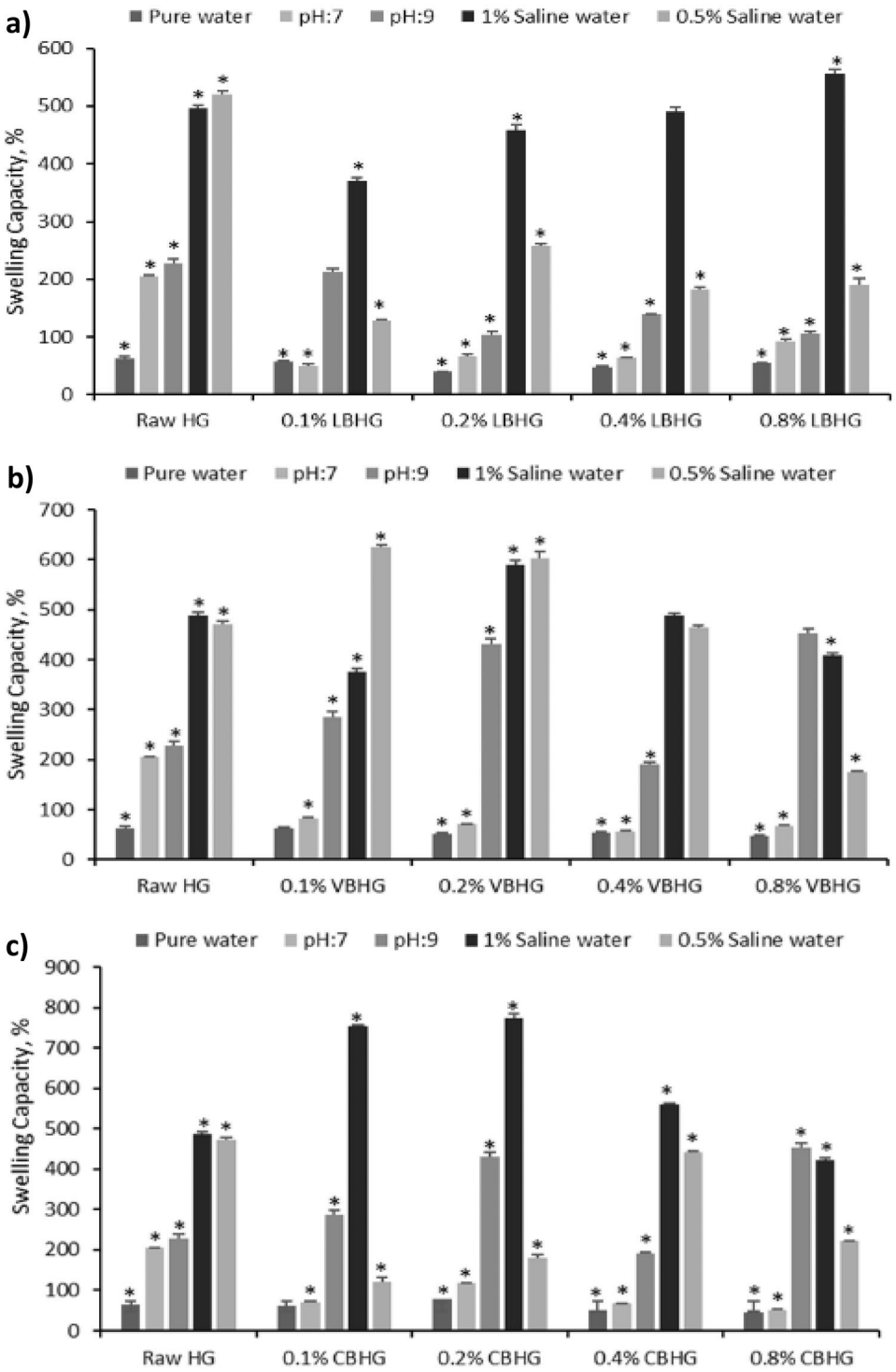

Fig. 4 Swelling capacities of **a** LBHGs, **b** VBHGs, and **c** CBHGs in pure water, pH 7.0 and pH 9.0 tap water, 1% (EC: 16.02 mS/cm) and 0.5% (EC: 7.80 mS/cm) saline water (*means statistically significant compared to control, $p < 0.05$)

capacity due to pH is caused by the electrostatic repulsion force between the carboxyl groups in the hydrogel. Therefore, the balance between the carboxylic groups in the hydrogel and the ion density in the solution in which the hydrogel is located is important in swelling capacity depending on pH value. The minimum and the maximum swelling capacity of CBHs was determined in the pure water and the 1% saline water, respectively. The CBHs showed good swelling capacity in saline water at the content of 0.1% and 0.2% of CB. It was observed that when the biochar content was increased, the swelling capacity decreased in 1% saline water, like in tap water at pH 9.0 (Fig. 4c) ($p < 0.05$).

All the results of the swelling capacity of synthesized hydrogels in different aqueous media showed similar trend

in literature studies. Zhang et al. (2020) showed some carboxylic groups (-COOH) ionized and the hydrogel bonds were weakened with increasing pH values; thus, the swelling capacity enhanced. In addition, according to Asy-Syifa et al. (2022), the hydrogels synthesis used SA-PVA polymers were dried to reach constant weight; thus, the polymer chains were in tight arrangement. After the drying process, the hydrogels were placed in aqueous media and the water molecules penetrate into the pores on the surface of hydrogels. With this process, the polymer chains were relaxed which caused the swelling (Asy-Syifa et al. 2022).

Figure 5 showed that the swelling capacity of synthesized biochar-doped hydrogels in soil–water mixture. It was determined that the LBHGs and VBHGs swelled as much as the raw hydrogels. In addition to the results, the 0.1% CB-doped hydrogels more swelled than the others, and the 0.8% CB-doped hydrogels had the minimum swelling capacity ($p < 0.05$). These experiments were conducted in tap water. When the results of free tap water and soil–water mixture compared, it was determined that the synthesized hydrogels swelled well in soil–water mixture. The reason of this results due to the increasing pH value of soil–water mixture aqueous media. As it can be seen in the Fig. 4, the increasing pH value and the electrostatic repulsion force caused the more swelling capacity.

3.3 Time-dependent swelling behavior of hydrogels

The swelling capacities were determined at different time intervals (5–320 min) to evaluate when the hydrogels reach the maximum swelling. In the literature, the swelling capacity of the synthesized hydrogels is conducted at different time depending on used polymers (Kipcak et al. 2014; Abdallah 2019; Asy-Syifa et al. 2022), so in this study the kinetic studies were conducted at 5 h. Results showed that LBGHs have faster swelling degrees compared to other biochar-hydrogel composites (Fig. 6). The maximum swelling capacity was determined at the 0.1% LB content in hydrogel (Fig. 6a) ($p < 0.05$) as 193.25%. In addition, all LBHGs had increasing swelling capacity with time, whereas for raw hydrogels the swelling capacity decreased with time. The degree of swelling of the raw hydrogels remained constant at 92.38% after 40 min. It was determined that the swelling capacity of LBHG decreased with increasing LB content in hydrogels and the minimum swelling capacity was found in hydrogels containing 0.8% LB. Hydrogels' ability to hold water is closely correlated to both the complexity of their chemical composition and complicated structures. Strong hydrogen connections between the -OH groups and NH_2 groups in PVA and SA, which generate these complicated structures, allow ionic complexes to form. It is possible to modify the water-holding capacity of these -OH bonds by placing the carboxyl groups of the biochar in the hydrogel. Hydrogels with high biochar content may form dense complicated structures, as was observed in this work, and their ability to hold water could be reduced. Since there may be longer carboxyl group chains in hydrogels with high biochar content, the hydrophobicity of the alkyl chain may also rise, lowering the hydrogels' ability to hold water (Kim et al. 2003; Sharma et al. 2015; Boran and Karakaya 2019). In addition, when the biochar content in hydrogel is well set, the swelling capacity can be increased (Li and Chen 2018b; Wu et al. 2021). Like in this study, 0.1% LB (as 193.2%), 0.1% VB (as 142.6%), and 0.2% CB (as 128.93%), content in hydrogels swelled well with increasing time compared to other contents of biochar and raw hydrogels (Fig. 6). The time-dependent swelling capacity of VBHGs showed similar tend with LBHGs. The swelling capacity decreased with increasing biochar content in hydrogels (Fig. 6b). In addition, CBHGs showed the maximum swelling capacity at 0.2% biochar content. The

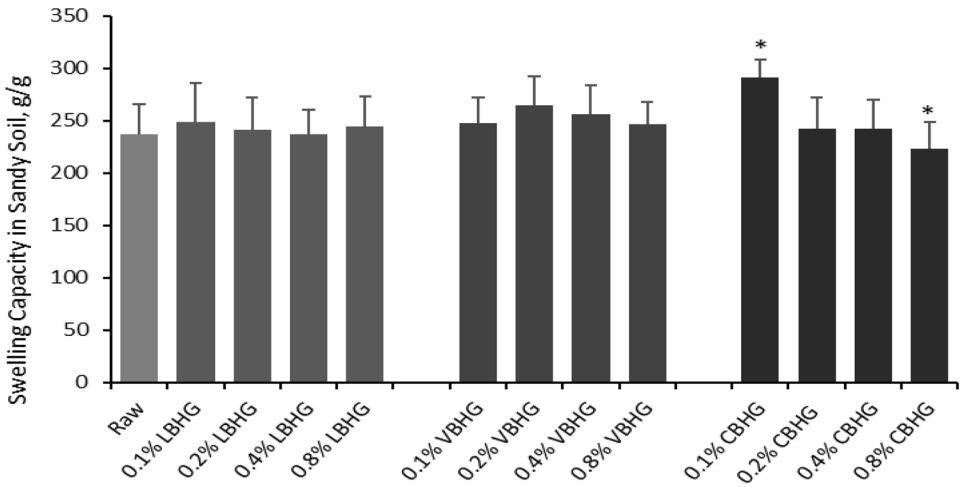

Fig. 5 Swelling capacity of **a** LBHGs, **b** VBHGs, and **c** CBHGs in loamy sand soil–water mixture (*means statistically significant compared to control, $p < 0.05$)

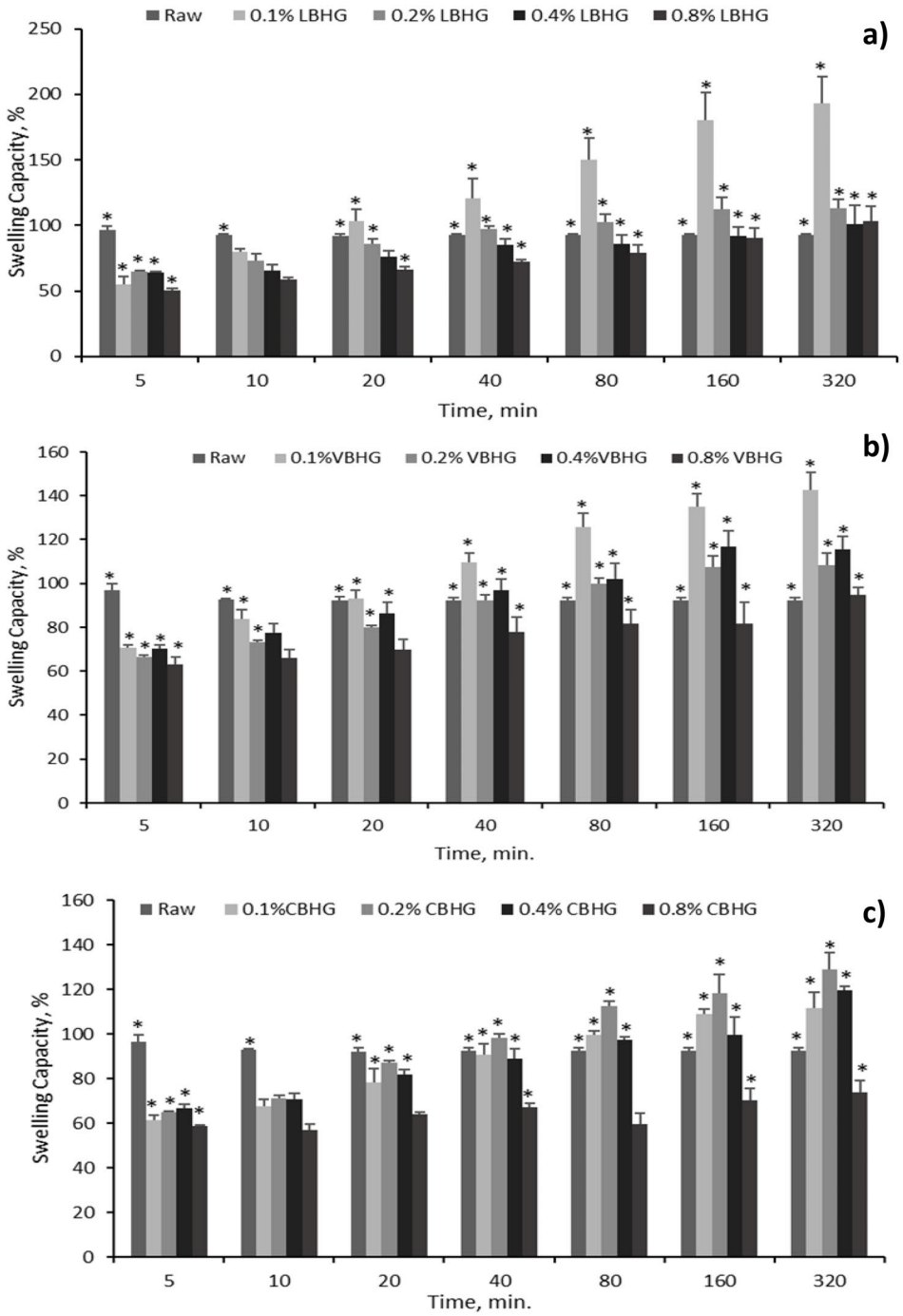

Fig. 6 Time-dependent swelling behavior of raw and biochar-doped hydrogels **a** LBHG, **b** VBHG, and **c** CBHG (*means statistically significant compared to control, $p < 0.05$)

swelling capacity was sorted as 0.2% (128.93%) > 0.4% (119.84%) > 0.1% (111.64%) > 0.8% (73.8%) biochar content for CBHGs (Fig. 6c).

The results in the literature were similar to this study. Bajpai and Shrivastava (2002) showed that the swelling capacity of synthesized hydrogels using poly-(ethylene glycol) and poly(acrylamide-co-styrene) swelled well with increasing time (up to 180 min). In addition, Das and Ghosh (2022) examined the swelling properties of pine resin biochar-added hydrogels and stated that the hydrogels showed a very high swelling property in the first 10 h. The authors indicated that this swelling behavior of biochar-doped hydrogels depended on the diffusion of water molecules and capillary properties of the hydrogels. The swelling mechanism was explained by the rapid rupture in the first 5 h, and then, the polymers continued to relax and swell until the 30th hour. Moreover, the most influential driving force in these swelling events is the relationship between the -$CONH_2$ functional groups and H-bonds with superior hydrophilic capacity (Das and Ghosh 2022).

3.4 Swelling curves

One of the crucial factors in the cross-linked hydrogels' characterization is swelling. The hydrogels of PVA/SA/BC composites were used in swelling tests at 25 °C ambient temperature. In order to determine swelling, 0.2 g of dried hydrogels was weighed and added to the beaker along with 100 mL of distilled water. Following the initial time being set ($t = 0$), the hydrogel weights were calculated after taking surface moisture readings at predetermined intervals. The swelling kinetics were then studied using the weights. Based on the data, the hydrogel swellings reached the equilibrium after about 160 min. The swelling kinetics were created using these data (Fig. 7).

3.5 Diffusion coefficients

The common laws used to describe water diffusion into the dried hydrogel and its diffusion type are known as Fick's laws (am Ende and Peppas 1997). Equation (3) was used to look into the mechanics of water diffusion into the swollen hydrogel. The logarithmic form of Eq. (3) was used to create the plots of Ln(F) versus ln (t), and these graphs were shown in Fig. 7. Table 4 contains the values of n, k, and regression coefficients that were determined from the slopes and intercepts of the plots of ln (F) against ln (t), respectively. Fick diffusion transport is defined by n and this value is used to determine the type of diffusion (Peppas and Brannon-Peppas 2013). The data from Eq. (3) refers to the

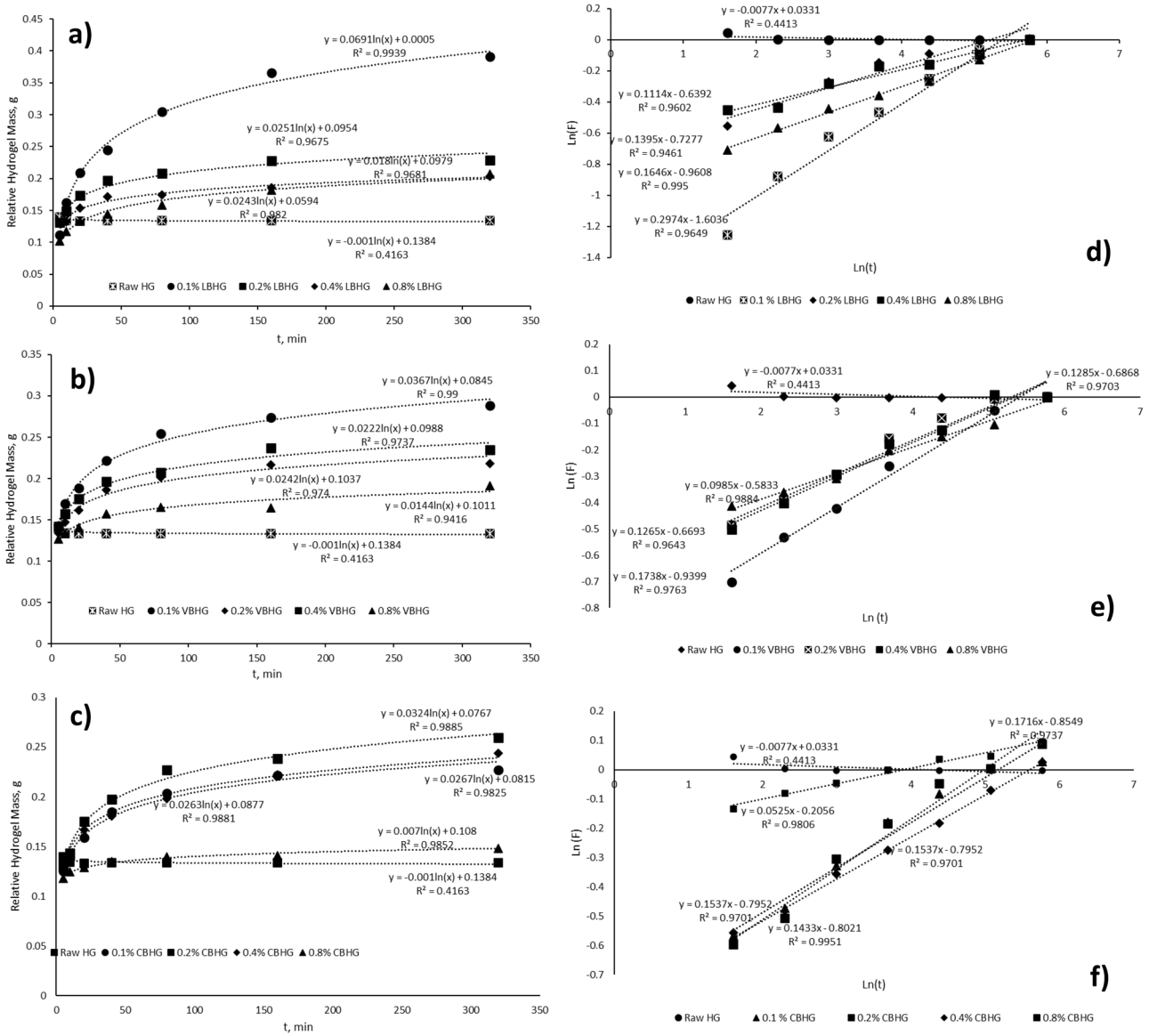

Fig. 7 Change of the relative hydrogel masses with time and their swelling kinetic curves **a** and **d** LBHG, **b** and **e** VBHG, **c** and **f** CBHG

Table 4 Swelling coefficient values of hydrogels

Coefficient	Raw HG	VBHG				CBHG				LBHG			
	0%	0.1%	0.2%	0.4%	0.8%	0.1%	0.2%	0.4%	0.8%	0.1%	0.2%	0.4%	0.8%
r (cm)	0.325	0.412	0.523	0.530	0.528	0.410	0.420	0.38	0.480	0.405	0.422	0.435	0.505
n	0.008	0.174	0.127	0.129	0.099	0.154	0.172	0.143	0.053	0.297	0.140	0.111	0.165
k	1.033	0.390	0.512	0.503	0.558	0.451	0.425	0.448	0.814	0.201	0.483	0.528	0.383
R^2	0.441	0.976	0.964	0.970	0.988	0.970	0.974	0.995	0.981	0.965	0.946	0.960	0.995
$D\times10^8$	1.36×10^{-69}	76.7	6.87	7.71	0.16	33.9	106.5	10.4	4.94×10^{-6}	2.17	4.46	0.64	50.7

rapid uptake of water diffusion by the hydrogels. It can be seen from the graphs showing the time-dependent swelling kinetics in Fig. 7 that the swelling reaches equilibrium, and the solvent mass enters the structure of the gels. Fickian diffusion and case II transport were found 0.008 for pure hydrogel without biochar, in the range of 0.099–0.174 for VBHG composite hydrogels containing 0.1–0.8% VB, in the range of 0.053–0.172 for CBHG composite hydrogels containing 0.1–0.8% CB, and in the range of 0.201–0.528 for LBHG composite hydrogels containing 0.1–0.8% LB, respectively.

Fick's rules are used to describe two types of diffusion: Fickian and non-Fickian diffusion. Non-Fickian diffusion does not abide by the Fickian laws, whereas Fickian diffusion does. The presence or absence of boundaries is the primary distinction between Fickian and non-Fickian diffusion; Fickian diffusion has no limits, but non-Fickian diffusion has a strong boundary separating the highly inflated zone from a dry, glassy region. According to this theory, there are some polymer systems where the borders between the swollen and un-swollen areas are crisp and move linearly over time. These swelling exponents (n) indicated that the transport of all superabsorbent polymers involved the non-Fickian diffusion character. The values for k varied between 0.390 and 0.558 for VBHG, 0.425 and 0.814 for CBHG, and 0.111 and 0.297 for LBHG. This value was obtained as 1.033 for raw HG. The high regression coefficient values (R^2) were obtained for all biochar-doped hydrogel (BHG) composites in the range of 0.946–0.995. One of the key variables used to characterize the hydrogel's swelling is its diffusion coefficient (D), which is determined using Eq. (4). Table 4 contains the hydrogels' determined values for the diffusion coefficient. The minimum D value was obtained for raw HG as 1.36×10^{-69}. The VBHG samples showed a highly variable D value depending on the % of biochar they contained. The lowest D value was obtained as 0.16 in the vine hydrogels containing 0.8% BC, while the highest D value (76.7) was reached in the 0.1% sample containing the lowest BC. Similarly, in composite hydrogels containing compost biochar (CB) in different ratios, the lowest diffusion coefficient was obtained in the hydrogel containing 0.8% biochar, while the highest D value (106.5) was reached in the hydrogel containing 0.2% compost biochar. Hydrogels containing leaf biochar (LB) showed a very different result. The highest D value (50.7) was obtained in the hydrogel (LBHG) containing 0.8% leaf biochar (LB), while the hydrogels containing 0.4% LB had the lowest diffusion coefficient (0.64). The sample with the highest diffusion coefficient was the hydrogels containing 0.2% compost biochar of all hydrogels.

3.6 Re-swelling properties

In agricultural applications or environmental treatment research, re-swelling capacity is a crucial measure to assess hydrogel's reusability. The re-swelling properties of hydrogels help the decreases in the irrigation period to reduce water loss by reducing the flow of irrigation water to underground and help the fight against drought depending on climate change. In this study, the re-swelling tests were conducted in 3 cycles to determine the possibility of water reabsorption, and the results showed that the hydrogels were swelled even after the 3rd cycle (Fig. 8). However, their re-swelling behavior showed that the biochar-doped hydrogels swelled less than the raw hydrogels (Fig. 8a–c). These results may be due to the easier relaxation of hydrophilic functional groups of PVA chains than biochars. Durpekova et al. (2020) proved that the synthesized hydrogels showed increased re-swelling behavior after 5 cycles. Our previous studies also showed that the re-swelling properties of biochar-doped hydrogels depend on the biochar species. It was determined that olive stone biochar-added hydrogels swelled well after three cycles, especially at 0.2% biochar content (Doğaroğlu and Uysal 2022), compared to raw hydrogels, while the swelling capacity of olive tree biochar-added hydrogels decreased with cycle periods (Doğaroğlu et al. 2022). The co-existence of many functional groups such as S = O, C = O, COOH, and C–OH in the biochar structure plays an important role in the re-swelling of biochar-doped hydrogels. Another parameter that plays an important role here is the amount of biochar in the hydrogel. When the amount of biochar in and on the surface of the hydrogel is low, the functional groups on the surface may combine and the hydrogels may swell more, while the excess biochar content may have the opposite effect (Wu et al. 2021). The main reason why the hydrogels swell less in the first cycle

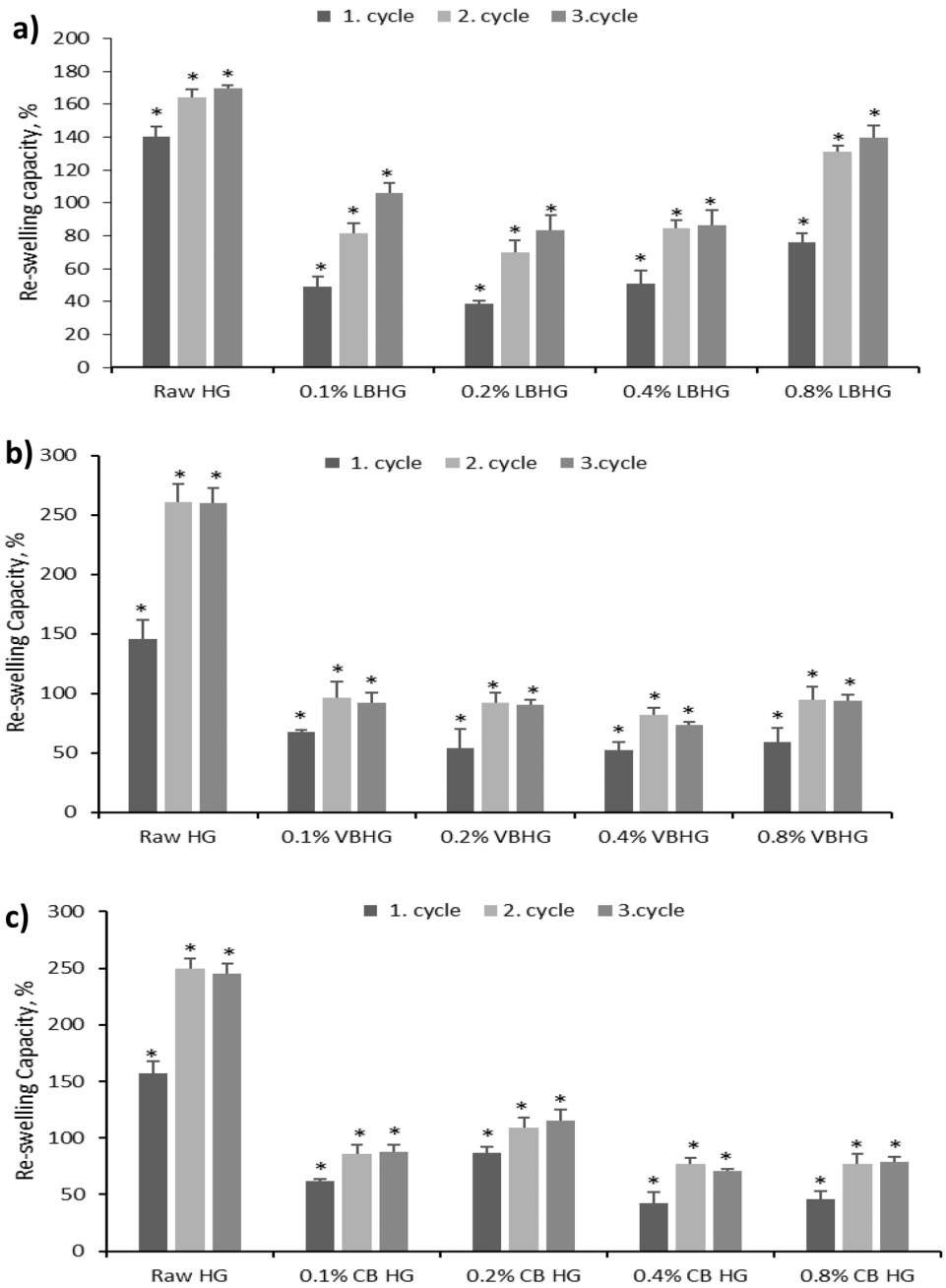

Fig. 8 Re-swelling capacity of **a** LBHGs, **b** VBHGs, and **c** CBHGs in pure water (*means statistically significant compared to control, $p < 0.05$)

compared to the last cycle may be due to the fact that water enters the pores on the surface of hydrogels (with capillary forces) in the first cycle and relaxes the hydrogel network. Then, the dried hydrogels may not leave the inner water (loosened networks) completely for the next cycles.

3.7 Seed germination

In arid or semi-arid regions, using hydrogels in the agricultural applications is very effective strategy due to having a good water retention capacity. Therefore, it is important to determine the impacts of hydrogels on growth parameters of plants and the studies on to determine the most effective hydrogels in agricultural fields (Li and Chen 2020). Biochar is one of the most fundamental materials to produce effective hydrogels since their porous structure, more cross-linking points, and thus increasing water retention capacity (Zhang et al. 2022). In this study, to evaluate the effectiveness and the phytotoxicological effects of synthesized raw and biochar-doped hydrogels in the seed germination process, germination experiments were conducted. Figure 9a depicts the interaction between wheat seed and raw hydrogel beads, and seedling images. Results showed that the addition of biochar in hydrogels was not significantly affected the seed germination of wheat at low concentration; however,

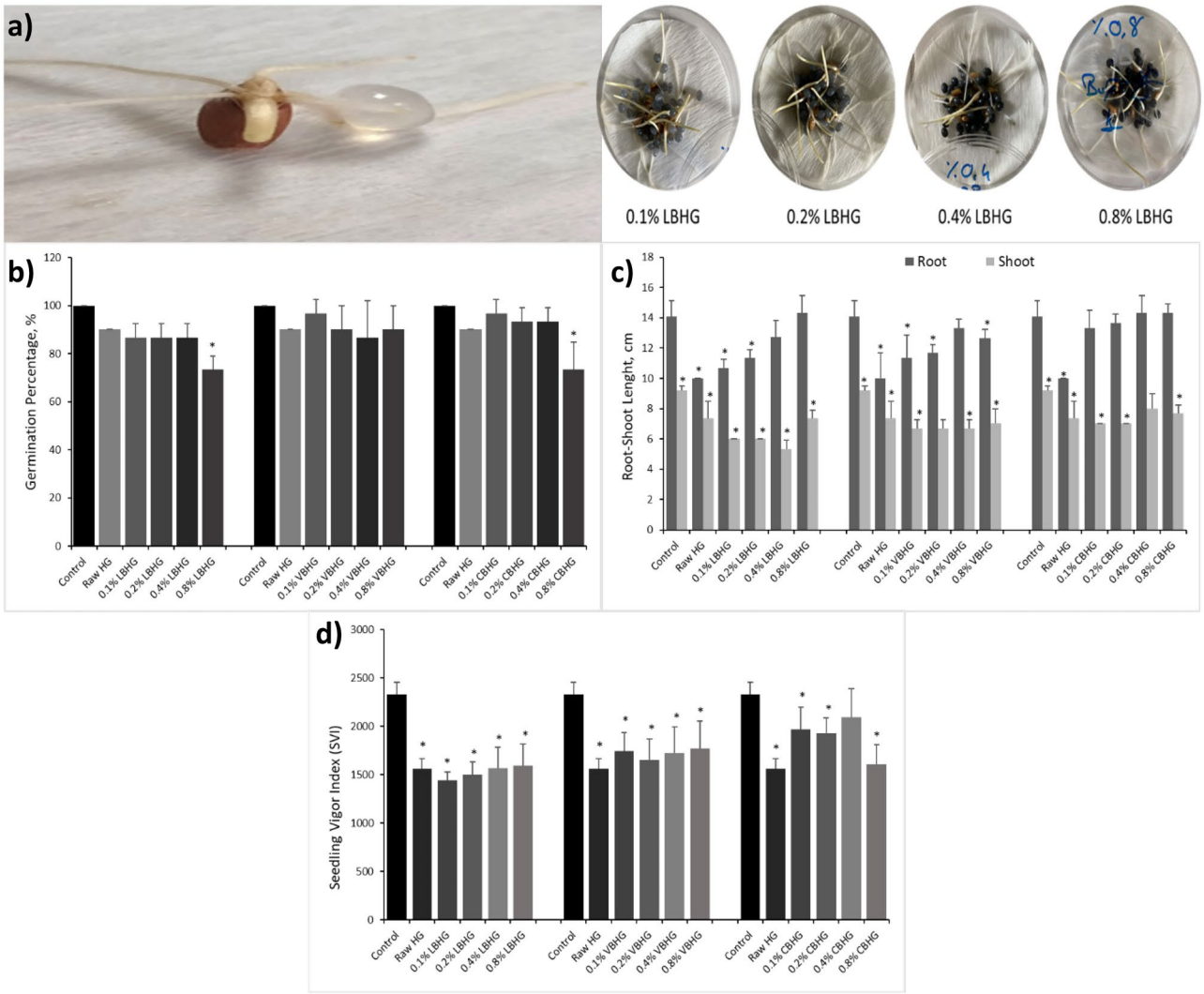

Fig. 9 **a** Images of wheat seed and Raw HG interaction, and seed germination, **b** seed germination percentage, **c** root-shoot length, and **d** seedling vigor index of wheat treated with different type and content of biochar-doped hydrogels (*means statistically significant compared to control, $p < 0.05$)

there was a threshold concentration for biochar (Fig. 9b). It was determined that if there was 0.8% LB and CB content in hydrogels, the seed germination percentage was significantly decreased compared to control. In addition, the vine pruning biochar-doped hydrogels positively affected the seed germination of wheat compared to raw hydrogels. However, these positive effects did not reach to control groups, like Zhang et al. (2022). Although the moisture can be enhanced with the hydrogels for the germination of seeds (Wu et al. 2021), the germination rate was not affected from this enhancement. In addition to these findings, the germination process was aided by the synthesized method, hydrogel content, and germination media, as demonstrated by Barajas-Ledesma et al. (2020), who found that cellulose-based hydrogels improved the germination index of radish seeds. The first organ that emerges with the start of germination is the roots (radicle) and the most important parameter for the rapid and healthy growth and development of the plant is root elongation. According to Fig. 9c, biochar addition to the hydrogels enhanced the root elongation; however, it was not statistically significant. It was determined that the CBHGs were positively affected the root elongation compared to other types of biochar-doped hydrogels (LBHG and VBHG) (Fig. 9c). Also, the minimum root and shoot length was determined at the raw hydrogel treatments. It was observed that the root length was increased with increasing biochar content in hydrogels, while the shoot length was negatively affected from the biochar content compared to control ($p < 0.05$) and raw hydrogel. Qin et al. (2022) showed that the cellulose-based hydrogels was effective that water treatments on root production by wheat after 21 days. Also, the authors showed that the cellulose-based hydrogels enhanced the root elongation of wheat compared to other treatments (raw hydrogel or free

water treatments). In generally, the roots are more sensitive to external materials than shoots. The findings based on our results showed that while the root elongation increased with increasing biochar content in hydrogels, the shoot elongation affected negatively from the presence of biochar in hydrogels. The maximum decreased in the shoot elongation was determined as 42.06%, 27.5%, and 23.91% in the LBHG, VBHG, and CBHG treatment, respectively (Fig. 9c). The biochars have good amount of C, N, and H content. Thus, these elements may affect the seedling growth parameters such as root-shoot elongation, leaves area, or chlorophyll content, and also the enzymatic processes. The minimum changes in the root and shoot elongation compared to control were determined compost biochar (CB) treatment. It was assumed that the elemental composition (C, N, H) was the most effective parameter in this change. The CB had more N and H content compared to vine pruning and leaf biochars (Table 3). However, based on our experience and this study, we can say that there was a threshold that the biochar-doped hydrogels positively affect the plant growth. It was determined that this threshold was generally 0.1–0.4% biochar content in hydrogels (Doğaroğlu and Uysal 2022; Doğaroğlu et al. 2022; Doğaroğlu 2023). In addition to the biochar content in hydrogel, the type of raw biomass which is produced biochar affects this threshold. Cao and Li (2021) investigated the effects of agar and activated carbon-doped hydrogels on rapeseed seedling growth parameters. The authors showed that increasing activated carbon (AC) content in agarose hydrogels increased the root and shoot length till the agar-AC ratio was 50%. All these hydrogel applications are not only effective in drought-related studies, but also can be considered as a promising application in soilless agricultural applications. The seedling vigor index (SVI) is related with the germination percentage and root-shoot elongation. The SVI is a parameter that if the seedling was in stress or not. Figure 9d showed the SVI decreased with hydrogel treatments compared to control groups. The minimum and the maximum SVI was determined at 0.1% LBHG treatment as 1443.33 and at the 0.4% CBHG treatment as 2090, respectively. The determined SVI values decreased compared to non-hydrogels groups (control). This result indicated that although hydrogel application did not show any negative effect on the seed germination stage, the SVI values decreased as it caused inhibition in the root-shoot elongation stage (Fig. 9d).

4 Conclusion

In this study, the swelling properties of hydrogels synthesized with different biochar species derived from leaf, vine pruning materials, and compost were evaluated. Five different aqueous media were used to determine the swelling characteristics of the hydrogels. The amount and types of biochar were found to be the most important parameters affecting the swelling capacity. The time-dependent behavior and swelling dynamics of the polymers were also investigated, revealing that these properties depended on the presence and type of functional groups and the surface of the hydrogel. The water transportation mechanism was determined to exhibit non-Fickian diffusion characteristics. The maximum swelling capacity was determined in 0.1% saline water for all the synthesized biochar-doped hydrogel types due to the salting-in effect. The re-swelling property of the hydrogels demonstrated their ability to swell even after multiple drying-swelling cycles, with biochar-doped hydrogels showing an improved swelling capacity. The maximum swelling efficiencies were determined for 0.2% LBHG as 117%, 0.2% VBHG as 67.3%, and 0.8% CBHG as 70.5% in the drying-swelling cycle. The seed germination test indicated no significant toxic effects of the synthesized biochar-doped hydrogels derived from compost, leaf, and vine pruning materials. However, root elongation tests revealed negative effects on roots for certain biochar types, while compost biochar-doped hydrogels showed no impact. It was concluded that compost biochar-doped hydrogels could be used in plant growth and germination phases, while the biochar types used in the study were not suitable for agricultural purposes. The study emphasized the importance of considering various parameters, such as polymer and biochar species and ratios, and evaluating eco-toxicological properties before using hydrogels, particularly in agricultural applications.

Acknowledgements This work was supported by TUBITAK (Project No: 122N055). The authors are grateful to The Scientific and Technological Research Council of Turkey (TUBITAK) for supports.

Data availability The datasets generated during and/or analyzed during the current study are available from the corresponding author on reasonable request.

Declarations

Conflict of interest The authors declare no competing interests.

References

Abdallah AM (2019) The effect of hydrogel particle size on water retention properties and availability under water stress. Int Soil and Water Conserv Res 7:275–285. https://doi.org/10.1016/j.iswcr.2019.05.001

Aleid S, Wu M, Li R, Wang W, Zhang C, Zhang L, Wang P (2022) Salting-in effect of zwitterionic polymer hydrogel facilitates atmospheric water harvesting. ACS Mat Lett 4:511–520. https://doi.org/10.1021/acsmaterialslett.1c00723

Al-Wabel MI, Al-Omran A, El-Naggar AH, Nadeem M, Usman AR (2013) Pyrolysis temperature induced changes in characteristics and chemical composition of biochar produced from *conocarpus* wastes. Bioresour Technol 131:374–379

Am Ende MT, Peppas NA (1997) Transport of ionizable drugs and proteins in crosslinked poly(acrylic acid) and poly(acrylic acid-co-2-hydroxyethyl methacrylate) hydrogels:II. Diffusion and release studies. J of Cont Release 48:47–56. https://doi.org/10.1016/S0168-3659(97)00032-1

An X, Yu J, Yu J, Tahmasebi A, Wu Z, Liu X, Yu B (2020) Incorporation of biochar into semi-interpenetrating polymer networks

through graft co-polymerization for the synthesis of new slow-release fertilizers. J Clean Prod 272:122731. https://doi.org/10.1016/j.jclepro.2020.122731

Armynah B, Tahir D, Tandilayuk M, Djafar Z, Piarah WH (2019) Potentials of biochars derived from bamboo leaf biomass as energy sources: effect of temperature and time of heating. Int J of Biomat Article ID 3526145. https://doi.org/10.1155/2019/3526145

Asy-Syifa N, Kusjuriansah, Waresindo WX, Edikresnha D, Suciati T, Khairurrijal K (2022) The study of the swelling degree of the PVA hydrogel with varying concentrations of PVA. IOP Pub: J of Physics: Conf Ser 2243:012053. https://doi.org/10.1088/1742-6596/2243/1/012053

Bajpai AK, Shrivastava M (2002) Swelling kinetics of a hydrogel of poly(ethylene glycol) and poly(acrylamide-co-styrene). J of App Poly Sci 85:1419–1428

Barajas-Ledesma RM, Patti AF, Wong VN, Raghuwanshi VS, Garnier G (2020) Engineering nanocellulose superabsorbent structure by controlling the drying rate. Coll and Surf A 600:124943

Boran F, Karakaya Ç (2019) Polyvinyl alcohol/CuO nanocomposite hydrogels: facile synthesis and long-term stability. J BAUN Inst Sci Technol 21(2):512–530. https://doi.org/10.25092/baunfbed.624392

Cao L, Li N (2021) Activated-carbon-filled agarose hydrogel as a natural medium for seed germination and seedling growth. Int J of Biol Macromol 177:383–391. https://doi.org/10.1016/j.ijbiomac.2021.02.097

Chen D, Liu D, Zhang H, Chen Y, Li Q (2015) Bamboo pyrolysis using TG-FTIR and a lab-scale reactor: analysis of pyrolysis behavior, product properties, and carbon and energy yields. Fuel 148:79–86

Cheng W-M, Hu X-M, Wang D-M, Liu G-H (2015) Preparation and characteristics of corn straw-Co-AMPS-Co-AA superabsorbent hydrogel. Polymers 7:2431–2445. https://doi.org/10.3390/polym7111522

Coates J (2000) Interpretation of infrared spectra, a practical approach. Encyclo of Analy Chem 12:10815–10837

Coates J (2006) Interpretation of infrared spectra, a practical approach. R.A. Meyers and M.L. McKelvy(ed) In: Encycl Anal Chem. https://doi.org/10.1002/9780470027318.a5606

Das SK, Ghosh GK (2022) Hydrogel-biochar composite for agricultural applications and controlled release fertilizer: a step towards pollution free environment. Energy 242:122977

Das SK, Ghosh GK, Avasthe R (2021) Applications of biomass derived biochar in modern science and technology. Env Tech Innov 21:101306. https://doi.org/10.1016/j.eti.2020.101306

Das SK, Ghosh GK, Avasthe R (2023) Application of biochar in agriculture and environment, and its safety issues. Biomass Conv and Bioref 13:1359–1369. https://doi.org/10.1007/s13399-020-01013-4

Dengre R, Bajpai M, Bajpai SK (2000) Release of vitamin B-12 from poly(N-vinyl-2- pyrrolidone)-crosslinked polyacrylamide hydrogels: a kinetic study. J Appl Polym Sci 76:1706–1714. https://doi.org/10.1002/(SICI)1097-4628(20000613)76:11%3c1706:AID-APP12%3e3.0.CO;2-W

Doğaroğlu ZG (2019) Role of EDDS and ZnO-nanoparticles in wheat exposed to TiO_2Ag-nanoparticles. Arch of Env Protec 45(4):78–83. https://doi.org/10.24425/aep.2019.130244

Doğaroğlu ZG (2023) Two different biochar-doped hydrogels affect the growth of arugula (Eruca vesicaria) under different irrigation period. J of Soils and Sedim 23:232–245. https://doi.org/10.1007/s11368-022-03383-w

Doğaroğlu ZG, Uysal Y (2022) Synthesis, swelling properties and effects on seed germination process of olive stone biochar-doped PVA/SA hydrogel. 2nd International Conference on Environment, Technology and Management 13–15 October, Niğde-Turkey

Doğaroğlu ZG, Uysal Y, Kalderis D (2022) Investigation of the viability of biochar-doped hydrogels in the fight against drought. In: Öz S (ed) Scientific research 2. Iksad Publications, Ankara, Turkey, pp 17–34

Du TS, Kang SZ, Zhang JH, Davies WJ (2015) Deficit irrigation and sustainable water-resource strategies in agriculture for China's food security. J Exp Bot 66(8):2253–2269. https://doi.org/10.1093/jxb/erv034

Durpekova S, Filatova K, Cisar J, Ronzova A, Kutalkova E, Sedlarik V (2020) A novel hydrogel based on renewable materials for agricultural application. Int J Polym Sci Article ID 8363418:1–13. https://doi.org/10.1155/2020/8363418

Feng D, Bai B, Wang H, Suo Y (2017) Novel fabrication of biodegradable superabsorbent microspheres with diffusion barrier through thermo-chemical modification and their potential agriculture applications for water holding and sustained release of fertilizer. J Agric Food Chem 65:5896–5907. https://doi.org/10.1021/acs.jafc.7b01849

Gaur VK, Gautam K, Sharma P, Gupta S, Pandey A, You S, Varjani S (2022) Carbon-based catalyst for environmental bioremediation and sustainability: updates and perspectives on techno-economics and life cycle assessment. Environ Res 209:112793. https://doi.org/10.1016/j.envres.2022.112793

Godiya CB, Cheng X, Li D, Chen Z, Lu X (2019) Carboxymethyl cellulose/polyacrylamide composite hydrogel for cascaded treatment/reuse of heavy metal ions in wastewater. J Hazard Mater 364:28–38. https://doi.org/10.1016/j.jhazmat.2018.09.076

Helmiyati, Aprilliza M (2017) Characterization and properties of sodium alginate from brown algae used as an ecofriendly superabsorbent. IOP Conf Ser: Mater Sci Eng 188:012019. https://doi.org/10.1088/1757-899X/188/1/012019

Isawi H (2020) Using zeolite/polyvinyl alcohol/sodium alginate nanocomposite beads for removal of some heavy metals from wastewater. Arabian J Chem 13:5691–5716. https://doi.org/10.1016/j.arabjc.2020.04.009

Jipa IM, Stoica A, Stroescu M, Dobre LM, Dobre T, Jinga S, Tardei C (2012) Potassium sorbate release from poly(vinyl alcohol)–bacterial cellulose films. Chem Pap 66(2):138–143. https://doi.org/10.2478/s11696-011-0068-4

Kang S, Xiao L, Meng L et al (2012) Isolation and structural characterization of lignin from cotton stalk treated in an ammonia hydrothermal system. Int J Mol Sci 13(11):15209–15226

Kim SJ, Lee KJ, Kim IY, Kim SI (2003) Swelling kinetics of interpenetrating polymer hydrogels composed of poly(vinyl alcohol)/chitosan. J of Macromol Sci Part A 40(5):501–510. https://doi.org/10.1081/MA-120019888

Kim S, Iyer G, Nadarajah A, Frantz JM, Spongberg AL (2010) Polyacrylamide hydrogel properties for horticultural applications. Int J Polym Anal Char 15(5):307–318. https://doi.org/10.1080/1023666X.2010.493271

Kipcak AS, Ismail O, Doymaz I, Piskin S (2014) Modeling and investigation of the swelling kinetics of acrylamide-sodium acrylate hydrogel. J of Chem Article ID:281063. https://doi.org/10.1155/2014/281063

Korbag I, Saleh SM (2016) Studies on the formation of intermolecular interactions and structural characterization of polyvinyl alcohol/lignin film. Int J Enviro Stud 73(2):226–235. https://doi.org/10.1080/00207233.2016.1143700

Laird D, Fleming P, Wang B, Horton R, Karlen D (2010) Biochar impact on nutrient leaching from a Midwestern agricultural soil. Geoderma 158(3–4):436–442. https://doi.org/10.1016/j.geoderma.2010.05.012

Lehmann J, Joseph S (2015) Biochar for environmental management: science. Techn and Implement Routle

Li S, Chen G (2018a) Using hydrogel-biochar composites for enhanced cadmium removal from aqueous media. Mat Sci & Eng Int J 2(6):294–298

Li S, Chen G (2018b) Thermogravimetric, thermochemical, and infrared spectral characterization of feedstocks and biochar

derived at different pyrolysis temperatures. Waste Manag 78:198–207. https://doi.org/10.1016/.05.048
Li S, Chen G (2020) Contemporary strategies for enhancing nitrogen retention and mitigating nitrous oxide emission in agricultural soils: present and future. Environ Dev Sustain 22(4):2703–2741. https://doi.org/10.1007/s10668-019-00327-2
Li L, Yang M, Lu Q, Zhu WK, Ma HQ, Dai LC (2019) Oxygen-rich biochar from torrefaction: a versatile adsorbent for water pollution control. Bioresour Technol 294:122142
Liu Z, Huang H (2016) Preparation and characterization of cellulose composite hydrogels from tea residue and carbohydrate additives. Carbohyd Polym 147:226–233. https://doi.org/10.1016/j.carbpol.2016.03.100
Liu X, Liao J, Song H, Yang Y, Guan C, Zhang Z (2019) A biochar-based route for environmentally friendly controlled release of nitrogen: urea-loaded biochar and bentonite composite. Sci Rep 9:1–12. https://doi.org/10.1038/s41598-019-46065-3
Ma B, Ma BL, McLaughlin NB, Mi J, Yang Y, Liu J (2020) Exploring soil amendment strategies with polyacrylamide to improve soil health and oat productivity in a dryland farming ecosystem: one-time versus repeated annual application. Land Degrad Dev 31:1176–1192. https://doi.org/10.1002/ldr.3482
Mary GS, Sugumaran P, Niveditha S, Ramalakshmi B, Ravichandran P, Seshadri S (2016) Production, characterization and evaluation of biochar from pod (Pisum sativum), leaf (Brassica oleracea) and peel (Citrus sinensis) wastes. Int J Recycl Org Waste Agricult 5:43–53. https://doi.org/10.1007/s40093-016-0116-8
Moretti MMS, Bocchini-Martins DA, Nunes CCC et al (2014) Pretreatment of sugarcane bagasse with microwaves irradiation and its effects on the structure and on enzymatic hydrolysis. Appl Energy 122:189–195
Osman AI, Fawzy S, Farghali M, Elgarahy AM, Fahim RA, Maksoud MIAA, Ajlan AA, Yousry M, Saleem Y, Rooney DW (2022) Biochar for agronomy, animal farming, anaerobic digestion, composting, water treatment, soil remediation, construction, energy storage, and carbon sequestration: a review. Environ Chem Lett 20:2385–2485. https://doi.org/10.1007/s10311-022-01424-x
Peppas NA, Brannon-Peppas L (2013) Water diffusion and sorption in amorphous macromolecular systems and foods. J of Food Eng 22(1–4):189–210
Peppas NA, Bures P, Leobandung W, Ichikawa H (2000) Hydrogels in pharmaceutical formulations. Europ J of Pharm and Biopharm 50:27–46
Putra RN, Lee YH (2020) Entrapment of micro-sized zeolites in porous hydrogels: Strategy to overcome drawbacks of zeolite particles and beads for adsorption of ammonium ions. Sep and Puri Tech 237:116351. https://doi.org/10.1016/j.seppur.2019.116351
Qin C-C, Abdalkarim SYH, Zhou Y, Yu H-Y, He X (2022) Ultra-high water-retention cellulose hydrogels as soil amendments for early seed germination under harsh conditions. J of Clean Prod 370:133602. https://doi.org/10.1016/j.jclepro.2022.133602
Rahman M, Zhu Q, Zhang Z, Zhou H, Peng X (2017) The roles of organic amendments and microbial community in the improvement of soil structure of a Vertisol. Appl Soil Ecol 111:84–93
Ray A, Banerjee A, Dubey A (2020) Characterization of biochars from various agricultural by-products using FTIR spectroscopy, SEM focused with image processing. IJAEB 13:423–430. https://doi.org/10.30954/0974-1712.04.2020.6
Sánchez-Borrego FJ, Barea de Hoyos-Limón TJ, García-Martín JF, Álvarez-Mateos P (2022) Production of bio-oils and biochars from olive stones: application of biochars to the esterification of oleic acid. Plants 11:70. https://doi.org/10.3390/plants11010070
Sharma K, Kumar V, Kaith BS, Kumar V, Som S, Kalia S, Swart HC (2015) Synthesis, characterization and water retention study of biodegradable gum ghatti-poly(acrylic acideaniline) hydrogels. Polym Degrad and Stability 111:20–31. https://doi.org/10.1016/j.polymdegradstab.2014.10.012
Shivakumara LR, Demappa T (2019) Synthesis and swelling behavior of sodium alginate/poly(vinyl alcohol) hydrogels. Turk J Pharm Sci 16(3):252–260. https://doi.org/10.4274/tjps.galenos.2018.92408
Siipola V, Tamminen T, Källi A, Lahti R, Romar H, Rasa K, Keskinen R, Hyväluoma J, Hannula M, Wikberg H (2018) Effects of biomass type, carbonization process, and activation method on the properties of bio-based activated carbons. Bio Res 13(3):5976–6002
Singh S, Kumar V, Dhanjal DS, Datta S, Bhatia D, Dhiman J, Samuel J, Prasad R, Singh J (2020) A sustainable paradigm of sewage sludge biochar: valorization, opportunities, challenges and future prospects. J Clean Prod 122259
Suresh R, Prasher SO, Patel RM, Qi Z, Elsayed E, Schwinghamer T, Ehsan AM (2018) Super absorbent polymer and irrigation regime effects on growth and water use efficiency of container-grown cherry tomatoes. Trans ASABE 61(2):523–531
Tan X, Liu Y, Zeng G, Wang X, Hu X, Gu Y et al (2015) Application of biochar for the removal of pollutants from aqueous solutions. Chemosphere 125:70–85
Thayumanavan N, Tambe P, Joshi G, Shukla M (2014) Effect of sodium alginate modification of graphene (by 'anion-π' type of interaction) on the mechanical and thermal properties of polyvinyl alcohol (PVA) nanocomposites. Comp Inter 21(6):487–506. https://doi.org/10.1080/15685543.2014.879512
Tu C, Wei J, Guan F, Liu Y, Sun Y, Luo Y (2020) Biochar and bacteria inoculated biochar enhanced Cd and Cu immobilization and enzymatic activity in a polluted soil. Environ Int 137:1–9. https://doi.org/10.1016/j.envint.2020.105576
Wang Z, Cao J, Wang J (2009) Pyrolytic characteristics of pine wood in a slowly heating and gas sweeping fixed-bed reactor. J Anal Appl Pyrolysis 84(2):179–184
Wang X, Feng JH, Cai YW, Fang M, Kong MG, Alsaedi A, Hayat T, Tan XL (2020) Porous biochar modified with polyethyleneimine (PEI) for effective enrichment of U(VI) in aqueous solution. Sci Total Environ 708:134575
Wu Y, Brickler C, Li S, Chen G (2021) Synthesis of microwave-mediated biochar-hydrogel composites for enhanced water absorbency and nitrogen release. Polym Test 93:106996. https://doi.org/10.1016/j.polymertesting.2020.106996
Zarzycki R, Modrzejewska Z, Nawrotek K (2010) Drug release from hydrogel matrices. Ecol Chem Eng S 17:117–136
Zhang Y, Tian X, Zhang Q, Xie H, Wang B, Feng Y (2022) Hydrochar-embedded carboxymethyl cellulose-g-poly(acrylic acid) hydrogel as stable soil water retention and nutrient release agent for plant growth. J of Biores and Bioprod 7:116–127. https://doi.org/10.1016/j.jobab.2022.03.003
Zhang W, Song J, He Q, Wang H, Lyu W, Feng H, Xiong W, Guo W, Wu J, Chen L (2020) Novel pectin based composite hydrogel derived from grapefruit peel for enhanced Cu (II) removal. J Hazard Mater 384:121445. https://doi.org/10.1016/j.jhazmat.2019.121445